Observation and simulation of hard x ray photoelectron diffraction to determine polarity of polycrystalline zinc oxide films with rotation domains

Jesse R. Williams,[1,2,a)] Igor Píš,[3,4] Masaaki Kobata,[3] Aimo Winkelmann,[5] Tomohiro Matsushita,[6] Yutaka Adachi,[1,2] Naoki Ohashi,[1,2,b)] and Keisuke Kobayashi[3,7]
[1]*International Center for Materials Nanoarchitectonics (MANA), National Institute for Materials Science (NIMS), 1-1 Namiki, Tsukuba, Ibaraki 305-0044, Japan*
[2]*NIMS Saint-Gobain Research Center of Excellence for Advanced Materials, NIMS, 1-2-1 Sengen, Tsukuba, Ibaraki 305-0047, Japan*
[3]*Synchrotron X-ray Station at SPring-8, NIMS, SPring-8, 1-1-1 Kouto, Sayo-cho, Sayo-gun, Hyogo 679-5198, Japan*
[4]*Department of Surface and Plasma Science, Faculty of Mathematics and Physics, Charles University, V Holešovičkách 2, Prague 8 18000, Czech Republic*
[5]*Max-Planck-Institut für Mikrostrukturphysik, Weinberg 2, D-06120 Halle (Saale), Germany*
[6]*Japan Synchrotron Radiation Research Institute (JASRI), SPring-8, 1-1-1 Kouto, Sayo-cho, Sayo-gun, Hyogo 679-5148, Japan*
[7]*Hiroshima Synchrotron Radiation Center, Hiroshima University, 2-313 Kagamiyama, Higashi-Hiroshima, Hiroshima 739-0046, Japan*

(Received 20 September 2011; accepted 3 January 2012; published online 13 February 2012)

X ray photoelectron diffraction (XPD) patterns of polar zinc oxide (ZnO) surfaces were investigated experimentally using hard x rays and monochromatized Cr $K\alpha$ radiation and theoretically using a cluster model approach and a dynamical Bloch wave approach. We focused on photoelectrons emitted from the Zn $2p_{3/2}$ and O 1*s* orbitals in the analysis. The obtained XPD patterns for the (0001) and $(000\bar{1})$ surfaces of a ZnO single crystal were distinct for a given emitter and polarity. Polarity determination of c-axis-textured polycrystalline ZnO thin films was also achieved with the concept of XPD, even though the in-plane orientation of the columnar ZnO grains was random. © *2012 American Institute of Physics*. [doi:10.1063/1.3682088]

I. INTRODUCTION

Zinc oxide (ZnO) is a semiconductor with the wurtzite-type structure. This structure exhibits spontaneous polarization along the c-axis, which is perpendicular to the basal plane, and this polarization is a result of the periodic stacking of anion and cation slabs at alternating interplanar spacings. The $<001>$ c-axis vector points toward the cation-terminated surface, and, conversely, the $<00\bar{1}>$ vector points toward the anion-terminated surface. Hence, these two polar surfaces are denoted as (0001) and $(000\bar{1})$ surfaces or simply c+ and c− surfaces. The spontaneous polarization of ZnO causes its anisotropic electronic structure,[1,2] chemical properties,[3] and mechanical properties[4] to be dependent on its polarity.

Nondestructive determination of crystallographic polarity is not a trivial process; some demonstrated methods include coaxial impact collision ion scattering spectroscopy (CAICISS),[5] scanning nonlinear dielectric microscopy,[6] and anomalous dispersion of x ray diffraction.[7] However, each of these methods has drawbacks. For example, CAICISS requires high-quality crystals with relatively large dimensions. Scanning nonlinear dielectric microscopy is only effective for local measurements and requires a standard sample for calibration. Anomalous dispersion of x ray diffraction requires knowledge of the film thickness and thickness uniformity. Convergent electron beam diffraction (CBED)[8] and chemical etching[3] are effective techniques for determining crystalline polarity, but both are destructive and CBED, particularly, is a local measurement using transmission electron microscopy.

On the way to developing a non-destructive and conventional technique for polarity determination, we have demonstrated that x ray photoelectron spectroscopy (XPS) is suitable for the polarity determination of ZnO crystals through the observation of valence band spectra[1,8,9] and x ray photoelectron diffraction (XPD) patterns.[10] In the valence band spectra, it is evident that a characteristic subpeak can be observed only from the (0001) face of ZnO and not from the $(000\bar{1})$ face. However, the origin of the subpeak found in the valence band spectra of the (0001) face is still vague. The XPD patterns generated using the photoelectrons emitted from the Zn $2p_{3/2}$ and O 1*s* core levels can be indexed by assuming strong forward scattering from the nearest neighbors, and the patterns are distinct for the (0001) and $(000\bar{1})$ faces. Thus, at present, XPD patterns are more reliable than valence band spectra for polarity determination of ZnO.

However, the reliability of the XPS/XPD results is limited by surface contamination or surface adsorption. Conventional XPS using soft x rays (SX), such as aluminum $K\alpha$ or magnesium $K\alpha$, has a probing depth on the order of 1 nm, because of the small inelastic mean free path (IMFP) of the photoelectrons. Although XPD patterns of ZnO can be observed with SX-XPS,[11,12] it is reasonable to argue that the reliability of SX-XPS may be affected by surface

a)Author to whom correspondence should be addressed. Electronic mail: Williams.Jesse@nims.go.jp.
b)Electronic mail: Ohashi.Naoki@nims.go.jp.

contamination. On the other hand, if hard x rays (HX) are used, XPS could be considered to be a bulk-sensitive technique,[13,14] because the IMFP is greater than 10 nm.[15] Recently, a laboratory-sized system using a chromium (Cr) $K\alpha$ source ($h\nu = 5417$ eV) has been developed,[16] and this system has previously demonstrated its ability to measure XPD patterns.[17] With the use of synchrotron radiation, it is possible to obtain reliable HX-XPD patterns;[10] moreover, Cr $K\alpha$ radiation is more accessible than synchrotron radiation.

There is currently a need for a polarity determination technique for polycrystalline films, because film properties depend on polarity, as mentioned above, and zinc oxide films on amorphous (glass and polymer) substrates are utilized in many applications, e.g., flat panel displays and solar cells. When depositing ZnO on glass or polymer substrates, ZnO films show a preferred orientation along the c-axis, but they are composed of in-plane rotation domains.[8] Therefore, it is necessary to develop a polarity determination technique for ZnO thin films with random in-plane orientation, because glass and polymer substrates are essential for future applications of ZnO thin films. Thus, we focused our investigation on XPD patterns of polycrystalline ZnO films. In the present study, we used Cr $K\alpha$ radiation to obtain bulk-sensitive XPD patterns of polycrystalline ZnO films deposited on glass substrates. These patterns were compared with those of single-crystal ZnO to explore the possibility for polarity determination of polycrystalline films with random in-plane orientation. In order to elucidate the observed results, we also performed theoretical simulations of the XPD patterns.

II. EXPERIMENTS

A. Samples

Single-crystal ZnO wafers from Tokyo Denpa Co. Ltd. (Tokyo, Japan) were used as a reference sample for the XPD measurements. The wafer surface was prepared by chemical mechanical polishing and had a nominal surface roughness of less than 1 nm. The polycrystalline samples were ZnO thin films grown on glass substrates by pulsed laser deposition (PLD). The films were textured such that the c-axis was parallel to the growth direction. The polarity was controlled with the use of dopants; the undoped film had a $(000\bar{1})$ surface and the film doped with 1 mol. % Al had a (0001) surface. Although these films were textured in the growth direction, they had a random in-plane orientation. Additional details about these films can be found elsewhere.[8]

The sample surfaces were pretreated prior to the XPD measurements, since the as-received or as-prepared samples were contaminated with carbon and oxygen due to exposure to air. In fact, the C 1*s* and O 1*s* core-level peaks ascribed to surface contamination were detected by conventional XPS measurements performed before pretreatment. The pretreatment, including heat treatment, decreased the relative intensity of the O 1*s* and C 1*s* peaks from adsorbates. The pretreatment procedure is described in detail in the supporting information.[18]

B. XPD measurements

The XPD measurements were made on a laboratory-developed system equipped with a monochromatized Cr $K\alpha$ x ray source, an objective lens with an effective acceptance angle of 70° and an angular resolution of 0.5°, and an electron energy analyzer with an angle-resolved measurement mode. More information about the instrument can be found elsewhere.[16]

To obtain the XPD patterns from the single-crystal samples, angular-resolved XPS spectra were taken, as presented in Fig. 1(a). The azimuthal angle (φ) dependence of the XPS profile was measured by rotating the sample from 0° to 60° in 2° intervals around the c-axis of ZnO, and the origin of φ was set to the $(11\bar{2}0)$ plane. At every φ angle, the polar angle (θ) dependence of the XPS profile was obtained in the θ region from 0° to 45° (the origin of θ was set to the surface normal direction, i.e., $<001>$ or $<00\bar{1}>$), utilizing the combination of the objective lens with a wide acceptance angle and the angle-resolved mode of the electron analyzer. The θ-dependent spectra were binned and averaged over every 1.18°. For all points in the θ–φ space, the respective core-level peaks were fit to a peak profile function to obtain the integrated peak intensity. Lastly, the obtained intensity distribution in θ–φ space was normalized by the θ–φ-dependent transmission function to remove instrumental contributions that affected the relative yield for photoelectron collection. Note that the instrumental transmission function was calibrated using amorphous silicon oxide.

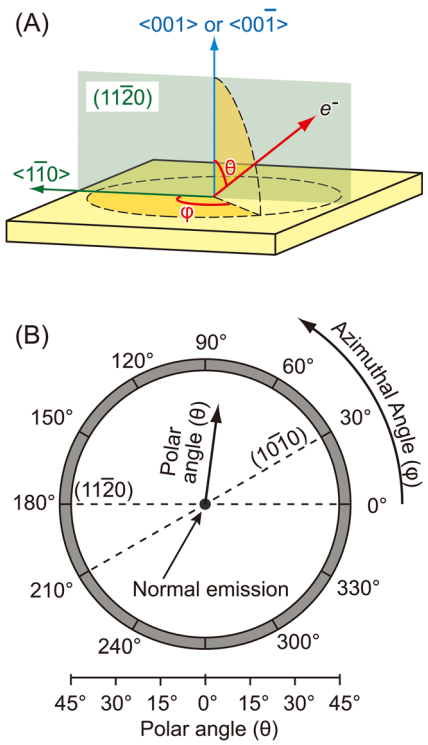

FIG. 1. (Color online) (a) Sample measurement geometry and (b) projection manner of the XPD intensity patterns. The polar angle (θ) is the out-of-plane angle measured from the normal emission, which is perpendicular to the sample surface, and the azimuthal angle (φ) defines the in-plane orientation. The azimuthal positions of the $(11\bar{2}0)$ and $(10\bar{1}0)$ planes are at $\varphi = 0°$ and 30°, respectively.

In this paper, the XPD patterns are plotted in a manner shown in Fig. 1(b), assuming sixfold symmetry of the XPD patterns. The radial direction corresponds to θ ranging from $\theta = 0$ at the center of the pattern to $\theta \approx 45°$ at the outer circumference, and the circumferential direction represents φ and covers 360° around the c-axis. Note that the presence of a sixfold symmetry was confirmed, as described in Sec. III. The signal-to-noise ratio was lower for the O 1*s* patterns, and there were greater fluctuations in the background signals when the samples were rotated. For this reason, the O 1*s* patterns were only measured over φ of 30°, and the measured patterns were mirrored before the sixfold symmetry was assumed.

For the polycrystalline thin films, only the θ dependence at a fixed φ angle was measured. Since these films had a random in-plane orientation, as shown schematically in Fig. 2, a complete θ–φ XPD pattern would have resulted in a ring pattern, as also illustrated in Fig. 2. Thus, one θ scan was sufficient to obtain all the relevant XPD data. The patterns were verified to be independent of φ by taking several θ scans at irregular φ intervals. The θ scans were then normalized by the transmission function to remove instrumental contributions in the same manner as the single-crystal samples.

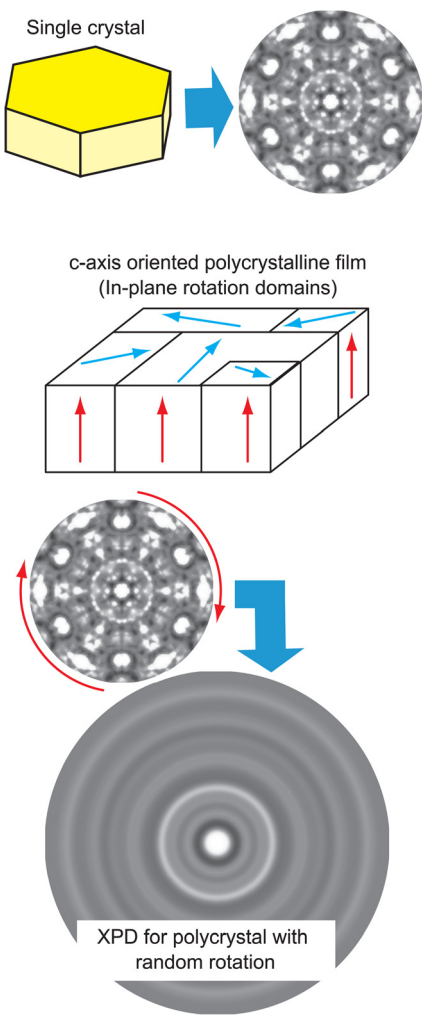

FIG. 2. (Color online) Schematic drawing of the expected XPD pattern of the c-axis–textured polycrystalline ZnO film with random in-plane orientation. Here, it is assumed that azimuthal averaging of the single-crystal XPD pattern produces the XPD pattern of the c-axis–textured film.

C. XPD simulations

Simulation of the XPD patterns was performed using two methods: a cluster model (CM) approach[19] and a dynamical Bloch wave (DBW) approach[20] for the identification and interrelation of the observed XPD patterns. The CM calculation code used in this study was developed by Matsushita *et al.*[19] for simulations of HX-XPD; the performance was optimized for an electron energy range of around 100 eV to several kiloelectronvolts.[21] Multiple scattering in the back scattering region was neglected in the CM code, but the forward scattering region was fully simulated for the reproduction of multiple scattering effects at a less expensive computational cost. In the present study, a cluster 3 nm in diameter was used, because of limited computational resources. Any structural relaxation at the surface was not considered, because the magnitude of the structural relaxation at the surface was not likely to be large[22,23] and small displacements of the top-most atoms was not expected to be a critical issue for HX-XPD utilizing the large IMFP of photoelectrons.

The DBW approach to electron diffraction,[20] namely Kikuchi-band theory or electron channeling, was also used in this study. The Bloch wave approach was used to calculate the electron probability density inside the crystal, and the modulation of this probability at the position of the photoelectron emitter described the diffraction by the crystal. This method has also previously been applied to the simulation of XPD patterns.[24,25] The advantage of the DBW method compared to the CM approach is that the computational demands are independent of the photoemission energy.

III. RESULTS AND DISCUSSION

A. Single-crystal sample

Figures 3 and 4 show the θ dependence of the normalized Zn $2p_{3/2}$ intensity for the (0001) and (000$\bar{1}$) faces, respectively. Here, the θ dependence is separated into subplots with a 60° periodicity (e.g., 0°, 60°, 120°, and 180°) to easily assess the in-plane symmetry. For both the (0001) and (000$\bar{1}$) faces, the line scans for a given 60° periodic subplot are self-similar, which shows that the XPD does indeed have sixfold symmetry. This result is significant, because it means a detailed measurement is only required between $\varphi = 0°$ and 60° to obtain a complete 360° XPD pattern.

Detailed XPD patterns from both the (000$\bar{1}$) and (0001) surfaces are shown in Fig. 5(a). These patterns are obtained using the normalized peak intensities of the Zn $2p_{3/2}$ and O 1*s* core levels and are plotted in the manner shown in Fig. 1(b). Bright areas on the pattern represent high measured photoelectron intensity, while dark areas indicate low photoelectron intensity. Figure 5(b) shows the measured patterns processed with linear interpolation and smoothing.

Figures 5(c) and 5(d) show the results of the XPD simulations using the DBW approach and CM approach, respectively. The measured Zn $2p_{3/2}$ XPD patterns show a clear distinction between the (000$\bar{1}$) and (0001) surfaces and a very good similarity with both the CM and the DBW simulations as a whole. In fact, clear agreement of the position of

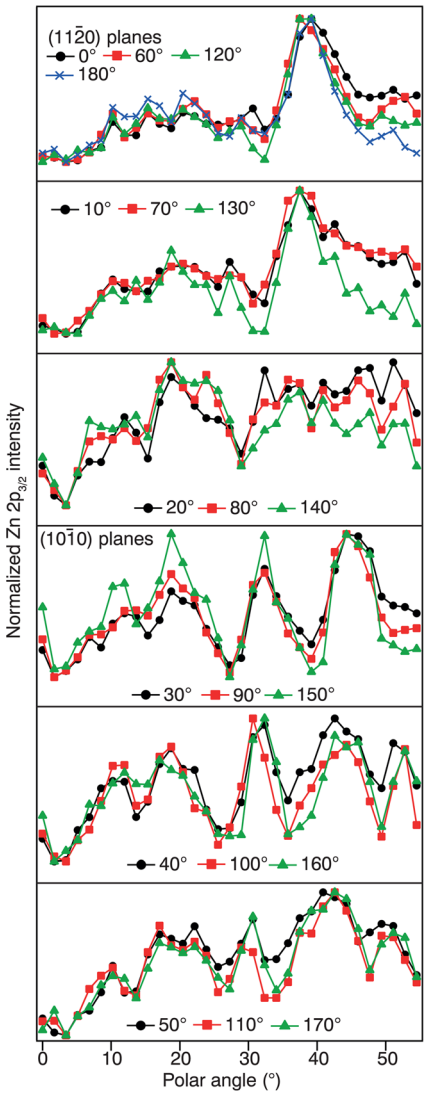

FIG. 3. (Color online) Polar angle (θ) dependency of core-level peak intensities taken from the (0001) ZnO surface. Profiles were taken for each azimuthal angle (φ) in steps of 10° and are grouped in φ intervals of 60° to illustrate the sixfold nature of the measurement.

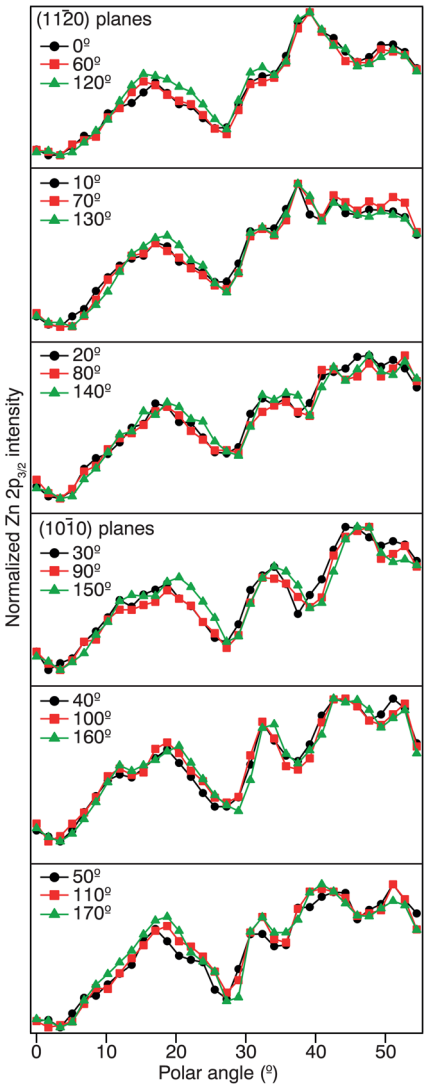

FIG. 4. (Color online) Polar angle (θ) dependency of core-level peak intensity taken from the (000$\bar{1}$) ZnO surface. Profiles were taken every 10° of azimuth (φ) and are grouped in φ intervals of 60° to illustrate the sixfold nature of the measurement.

the dominant features in the patterns was confirmed, and some of the predicted finer features are even present in the measured patterns. Thus, we can conclude that the observed variation of the XPS intensity in the θ–φ space was mostly due to photoelectron diffraction phenomena.

Very precise Kikuchi patterns are observed clearly in the DBW simulations. This is due to the bulk nature of the Bloch waves, which have long-range interference in the 2D channels of the atomic columns in the crystal. In the CM simulations, these Kikuchi patterns are not well reproduced, because the cluster size was too small. The CM simulation results resemble the experimental XPD patterns, although the cluster size used in this study was smaller than the IMFP of the photoelectrons. Insufficient angular resolution is a possible reason for the similarity between observed pattern and the simulation using the CM method.

The O 1*s* patterns are also corroborated by the simulated patterns. The major features are in the same position in both the measured and simulated patterns. Furthermore, a clear distinction between the (000$\bar{1}$) and (0001) polarities can be seen. Therefore, the intensity variation of the O 1*s* emission in the θ–φ space was also ascribed to XPD behavior, as was the Zn $2p_{3/2}$. However, the resolution of the O 1*s* intensity-measured patterns is significantly lower than that of the measured Zn $2p_{3/2}$ patterns. The difference in quality is largely due to their respective signal-to-noise ratios, because the intensity of the Zn $2p_{3/2}$ peak is over 5 times greater than that of the O 1*s* intensity and/or the evaluation of the peak intensity due to the O 1*s* component of the adsorbing matter is recorded with less accuracy. Although the resolution was not as high as we expected, the O 1*s* intensity pattern in the θ–φ space can also be used as a measure to identify the (0001) and (000$\bar{1}$) faces.

In relation to the discussion of the polycrystalline XPD patterns, we discuss the presence of a dark ring at $\theta \approx$ 26–27° in the XPD patterns for Zn $2p_{3/2}$ (000$\bar{1}$) and O 1*s* (0001), as indicated by the arrows in Fig. 5. Comparing the θ dependence shown in Figs. 3 and 4, the intensity minimum at $\theta \approx$ 26–27°, corresponding to the dark ring shown in Fig. 5, was more significant for the Zn $2p_{3/2}$ intensity for the

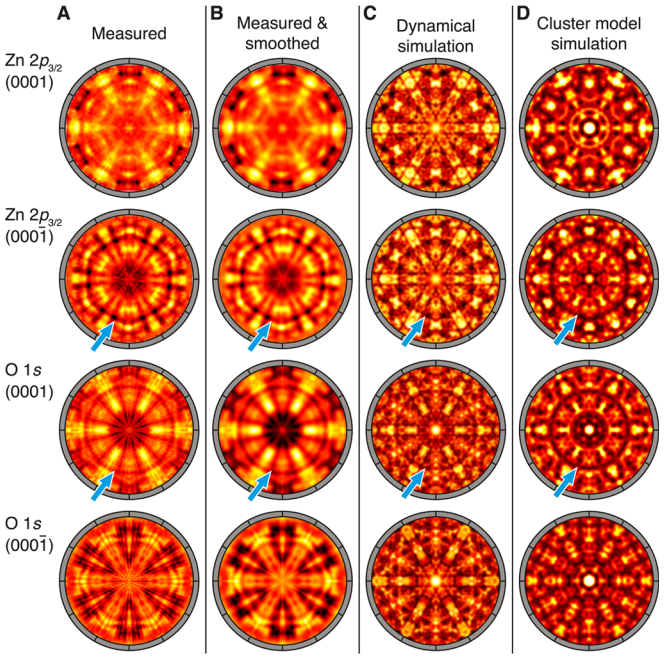

FIG. 5. (Color online) (a) XPD patterns as-measured, (b) interpolated and smoothed measured patterns, (c) dynamical Bloch wave simulations, and (d) cluster model simulations. These patterns were produced in the manner shown in Fig. 1(b). The arrows indicate the presence of a dark ring at around $\theta \approx 26$–$27°$.

$(000\bar{1})$ face than the (0001) face. This feature will be discussed in detail in Subsection III B.

B. Polycrystalline sample

The θ dependency of the Zn $2p_{3/2}$ and O 1s intensities of the polycrystalline samples are shown in Fig. 6, accompanied by the results of the CM and DBW simulations. Note that the theoretical θ dependencies of the XPD profiles were obtained by integrating the simulated intensity profiles shown in Fig. 5 over a φ range of 0°–360° at specific θ angles using the concept illustrated in Fig. 2. The most notable feature found in Fig. 6 was the presence of an intensity minimum around $\theta \approx 26$–$27°$ in the Zn $2p_{3/2}$ $(000\bar{1})$ and O 1s (0001) profiles. These diffraction minima are confirmed in both simulations and also correspond to the dark ring features found in the respective Zn $2p_{3/2}$ $(000\bar{1})$ and O 1s (0001) single-crystal XPD patterns (Fig. 5). Since this particular feature is ring shaped in the single-crystal XPD patterns, the azimuthal averaging resulting from the in-plane grain rotation does not weaken it in the polycrystalline intensity profiles. Therefore, the distinct intensity minimum found around $\theta \approx 26$–$27°$ in the polycrystalline intensity profiles is suitable for polarity determination.

The origin of the dark ring feature in the single-crystal XPD pattern (Fig. 5) and the intensity minima found in the polycrystalline XPD patterns (Fig. 6) are related to the relative cation-anion positions. Figures 7(a) and 7(b) show typical examples of the geometrical relationship between the photoelectron emitter and scatterer around the A-terminated surface of the wurtzite-type lattice composed of A and B elements. The lines in Fig. 7(a) shows emitter-scatterer combinations of the $(11\bar{2}0)$ plane, where an A atom contributes as the scatterer,

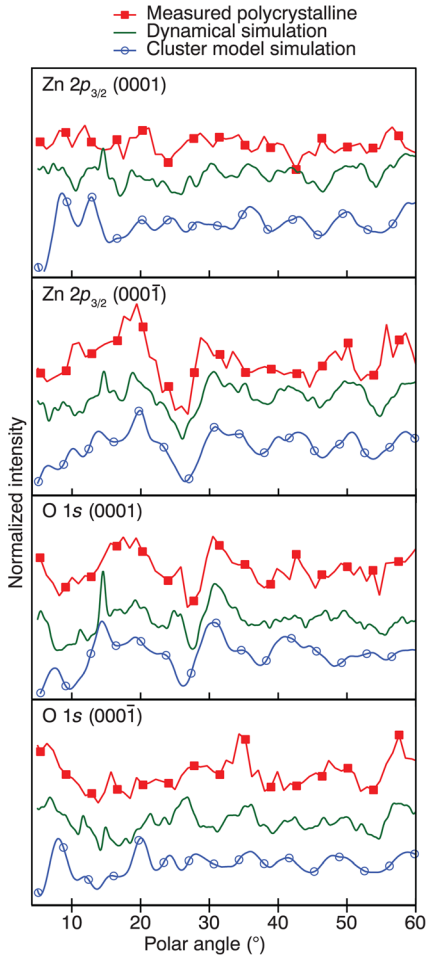

FIG. 6. (Color online) Polar angle (θ) dependency of the core-level peak intensities from the polycrystalline films. The measured data is shown in the top curve of each plot followed by the dynamical Bloch wave simulations and cluster model simulations, respectively. The strongest polarity-identifying features are the diffraction minima found at $\theta \approx 26$–$27°$ for the Zn $2p_{3/2}$ $(000\bar{1})$ and O 1s (0001) θ profiles.

and Fig. 7(b) shows that of the $(10\bar{1}0)$ plane, where a B atom contributes as the scatterer. The other configurations, a B scatterer of the $(11\bar{2}0)$ plane and an A scatterer of the $(10\bar{1}0)$ plane, are not shown here, but we considered all the emitter-scatterer combinations of both planes. A summary of the emitter-scatterer relationships of the $(10\bar{1}0)$ and $(11\bar{2}0)$ planes is shown in Fig. 7(c). As a result, the emitter-scatterer vector around $\theta \approx 26$–$27°$ is absent for the combination of a B emitter with an A scatterer for an A-terminated surface. This explains the significant diffraction minima around $\theta \approx 26$–$27°$ in the Zn $2p_{3/2}$ $(000\bar{1})$ and O 1s (0001) patterns. Therefore, we conclude that the distinct minimum found in the θ dependence of the core-level intensity profiles is a useful fingerprint for the determination of the polarity in the c-axis–textured polycrystalline films.

It should be considered why some of the calculated and observed profiles are not very self-similar. For example, features common to both simulated Zn $2p_{3/2}$ (0001) profiles, shown in Fig. 6, were lost in the respective observed profile. The similarity between the simulations and observation was better for both intensity profiles from the $(000\bar{1})$ face. In fact, in the intensity profile for O 1s $(000\bar{1})$, the intensity maxima

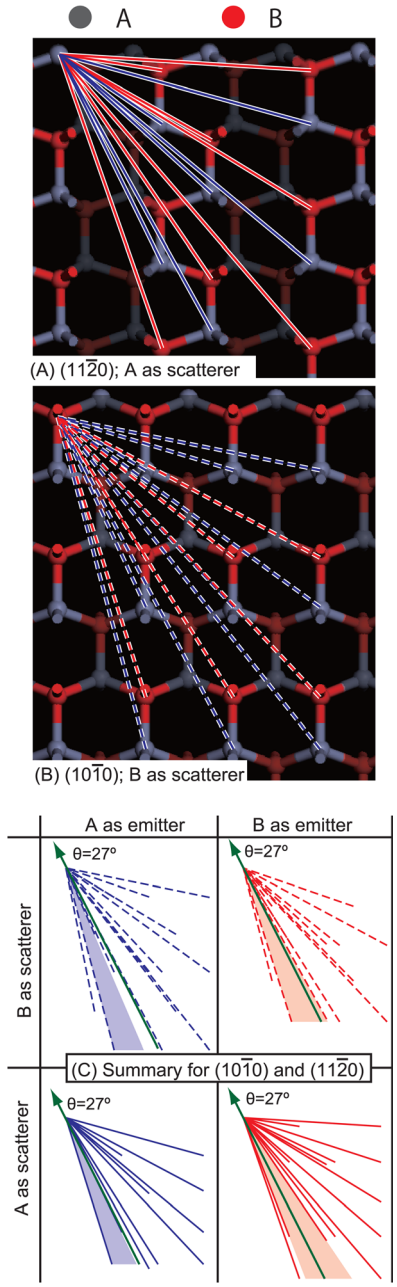

FIG. 7. (Color online) Typical geometrical relationship between the emitter and scatterer in a wurtzite-type lattice composed of A and B elements. (a) The A element as the scatterer and the B element as the emitter in the (11$\bar{2}$0) plane, (b) the B element as the scatterer and the A element as the emitter in the (10$\bar{1}$0) plane, and (c) a summary of emitter-scatterer vectors in the (11$\bar{2}$0) and (10$\bar{1}$ 0) planes. The shaded area in (c) indicates the angular range where the emitter-scatter combination is absent.

around $\theta \approx 35$, 49, and 58° seen in the simulated profiles could also be seen in the measured profile. The discrepancy between the observed and calculated (0001) polycrystalline intensity profiles may be due to the low crystallinity of the sample and small columnar grain size. The (0001) face film was obtained by heavy doping, which resulted in low crystallinity. In contrast, the (000$\bar{1}$) face, the undoped film, had a relatively high crystallinity and large grain size. Thus, low crystallinity is one possible reason to explain why there is less similarity between the observed and simulated profiles for the (0001) face.

In addition to the crystallinity issues, we assume that the very small columnar size of the heavily Al-doped film is also a reason for less consistency between simulation and observation. In the polycrystalline samples, there is a possibility that a photoelectron emitted in a grain is scattered by the neighboring grain with a different in-plane orientation. The probability of such intergrain scattering becomes higher with a decrease of the grain size. Thus, another possible reason for the discrepancy between the observed and calculated results for polycrystalline samples is the high probability of intergrain scattering due to the very small grain size.

Although we speculate that low crystallinity and small grain size are behind the discrepancy between the observed and calculated profiles from the (0001) polycrystalline film, for a complete assessment, a polarity-controlled (0001) polycrystalline film of high crystallinity is required. However, at present, it is very difficult to obtain such high quality films. Further investigations are still needed for a complete understanding of the XPD profiles of polycrystalline samples, but it is, at least, evident that the distinct feature found at $\theta \approx$ 26–27° can be used for the polarity determination of polycrystalline films. Indeed, this feature could be seen, even for films with very low crystallinity.

C. Polarity determination of wurtzite-type lattice by XPD

For the purpose of polarity determination in c-axis–textured polycrystalline ZnO thin films, the θ dependency of the O 1*s* and Zn $2p_{3/2}$ core-level intensities are the clearest indicators of the polarity. Importantly, it also signals that polarity determination of textured polycrystalline thin films is possible using XPD. We used HX-XPS here to demonstrate the polarity determination of a polycrystalline film by XPD. However, these results should be reproducible with XPD measurements using a conventional spectrometer and Mg $K\alpha$ or Al $K\alpha$ radiation, since the θ-dependent core-level peak intensity variation occurs via the XPD mechanism. Prior to this study, Zhang *et al.*[26] reported that comparing the (Zn 2*p*)/(O 1*s*) intensity ratio at $\theta = 0$ and 70° is a possible way to determine the polarity of c-axis–textured polycrystalline ZnO. However, obtaining the correct integrated intensity at $\theta = 70°$ is technically difficult because of surface contamination. For polarity determination, use of the XPD technique would seem to be easier than the method of Zhang *et al.*, because the polarity fingerprint can be obtained at a lower θ range ($\theta \approx$ 26–27°). It should also be noted that overlap of the peaks from Auger transitions with the XPS peaks is a potential cause for difficulty in the evaluation of the correct integrated peak intensity. In HX-XPS spectra, the relevant Auger electron peaks are absent. Thus, a rather smooth background in the HX-XPS spectra should be another merit for the polarity determination via the XPD mechanism. Furthermore, it has to be pointed out that this technique should be appropriate for the polarity determination of other wurtzite-type semiconductors, such as (Zn,Mg)O alloys and GaN, because the crystal structure determines the XPD profiles.

IV. CONCLUSION

In this work, we have shown that it is possible to determine crystallographic polarity nondestructively using XPD excited with hard x rays generated from a laboratory system. Moreover, it is possible to distinguish the (0001) and $(000\bar{1})$ faces of both single-crystal and c-axis–textured polycrystalline wurtzite-type ZnO. Two characteristics of HX-XPS, namely the absence of Auger peaks and bulk-sensitivity, enabled us to determine the crystalline polarity relatively easily as compared to other methods. We expect that this technique will contribute to the development of science and technology for wurtzite-type semiconductors, especially by solving issues related to crystalline polarity.

ACKNOWLEDGMENTS

Part of this study was supported by the World Premier International Research Center (WPI) Initiative (MANA-NIMS) of the Ministry for Education, Culture, Sports, Science and Technology (MEXT), Japan; a Grant-in-Aid for Scientific Research (Nos. 19053008 and 20246007) from the Japan Society for Promotion of Science (JSPS); a Sakura Fund from JSPS for French-Japan bilateral exchange; a grant for the Development of Systems and Technology for Advanced Measurement and Analysis promoted by the Japan Science and Technology Agency (JST), Japan; and the JST "Sentan" project. I.P. thanks the Czech Grant Agency for the research support (No. 202/09/H041). The authors also acknowledge helpful discussions with Dr. Hideki Yoshikawa of NIMS.

[1]N. Ohashi, Y. Adachi, T. Ohsawa, K. Matsumoto, I. Sakaguchi, H. Haneda, S. Ueda, H. Yoshikawa, and K. Kobayashi, Appl. Phys. Lett. **94**, 122102 (2009).
[2]N. Ohashi, K. Kataoka, T. Ohgaki, I. Sakaguchi, H. Haneda, K. Kitamura, and M. Fujimoto, Jpn. J. Appl. Phys. **46**, L1042 (2007).
[3]N. Ohashi, K. Takahashi, S. Hishita, I. Sakaguchi, H. Funakubo, and H. Haneda, J. Electrochem. Soc. **154**, D82 (2007).
[4]E. Barthel, O. Kerjan, P. Nael, and N. Nadaud, Thin Solid Films **473**, 272 (2005).
[5]H. Maki, N. Ichinose, S. Sekiguchi, N. Ohashi, T. Nishihara, H. Haneda, and J. Tanaka, Jpn. J. Appl. Phys. **38**, 2741 (1999).
[6]S. Kazuta, Y. Cho, H. Odagawa, and M. Kadota, Jpn. J. Appl. Phys. **39**, 3121 (2000).
[7]H. Tampo, P. Fons, A. Yamada, and K. Kim, **301–302**, 358 (2005).
[8]Y. Adachi, N. Ohashi, T. Ohgaki, T. Ohnishi, I. Sakaguchi, S. Ueda, H. Yoshikawa, K. Kobayashi, J. R. Williams, and T. Ogino, Thin Solid Films **519**, 5875 (2011).
[9]J. R. Williams, H. Yoshikawa, S. Ueda, Y. Yamashita, K. Kobayashi, Y. Adachi, H. Haneda, T. Ohgaki, H. Miyazaki, T. Ishigaki, and N. Ohashi, "," Appl. Phys. Lett. (in press).
[10]J. R. Williams, M. Kobata, I. Pis, E. Ikenaga, T. Sugiyama, K. Kobayashi, and N. Ohashi, Surf. Sci. **605**, 1336 (2011).
[11]K. H. Ernst, A. Ludviksson, R. Zhang, J. Yoshihara, and C. T. Campbell, Phys. Rev. B **47**, 13782 (1993).
[12]J. Yoshihara, J. M. Campbell, and C. T. Campbell, Surf. Sci. **406**, 235 (1998).
[13]K. Kobayashi, Nucl. Instrum. Methods Phys. Res. A **601**, 32 (2009).
[14]K. Kobayashi, M. Yabashi, Y. Takata, T. Tokushima, S. Shin, K. Tamasaku, D. Miwa, T. Ishikawa, H. Nohira, T. Hattori, Y. Sugita, O. Nakatsuka, A. Sakai, and S. Zaima, Appl. Phys. Lett. **83**, 1005 (2003).
[15]C. J. Powell and A. Jablonski, *NIST Electron Inelastic-Mean-Free-Path Database – Version 1.2* (National Institute for Standards and Technology, Gaithersburg, MD, 2010).
[16]M. Kobata, I. Pis, H. Iwai, H. Yamazui, H. Takahashi, M. Suzuki, H. Matsuda, H. Daimon, and K. Kobayashi, Anal. Sci. **26**, 227 (2010).
[17]I. Pıš, M. Kobata, T. Matsushita, H. Nohira, and K. Kobayashi, Appl. Phys. Express **3**, 56701 (2010).
[18]See supplementary material at http://dx.doi.org/10.1063/1.3682088 for sample surface pretreatment procedure.
[19]T. Matsushita, F. Matsui, H. Daimon, and K. Hayashi, J. Electron Spectrosc. Relat. Phenom. **178**, 195 (2010).
[20]A. Winkelmann, C. S. Fadley, and F. J. Garcia de Abajo, New J. Phys. **10**, 113002 (2008).
[21]A. Uesaka, K. Hayashi, T. Matsushita, and S. Arai, Phys. Rev. Lett. **107**, 045502 (2011).
[22]H. Maki, N. Ichinose, N. Ohashi, H. Haneda, and J. Tanaka, Surf. Sci. **457**, 377 (2000).
[23]B. Meyer and D. Marx, Phys. Rev. B **67**, 035403 (2003).
[24]A. Winkelmann, B. Schröter, and W. Richter, Ultramicroscopy **98**, 1 (2003).
[25]A. Winkelmann, B. Schröter, and W. Richter, Phys. Rev. B **69**, 245417 (2004).
[26]L. Zhang, D. Wett, R. Szargan, and T. Chasse, Surf. Interface Anal. **36**, 1479 (2004).